Micron 188 (2025) 103745

Contents lists available at ScienceDirect

Micron

journal homepage: www.elsevier.com/locate/micron

Short communication

Practical considerations for plunge freezing samples over 40 °C for Cryo-EM

Iain Harley [a], Francesca Mazzotta [a], Xhorxhina Shaulli [b], Frank Scheffold [b], Katharina Landfester [a], Ingo Lieberwirth [a,*]

[a] Max Planck Institute for Polymer Research, Ackermannweg 10, Mainz 55128, Germany
[b] Department of Physics, University of Fribourg, Chemin du Musée 3, Fribourg 1700, Switzerland

ARTICLE INFO

Keywords:
Cryo-EM
Temperature-responsive polymers
Sample vitrification
Plunge freezing

ABSTRACT

Cryo-EM is now an established tool for examining samples in their native, hydrated states—a leap made possible by vitrification. Utilising this sample preparation method to directly visualise temperature-responsive samples allows for deeper insights into their structural behaviours under functional conditions. This requires samples to be plunge-frozen at elevated temperatures and presents additional challenges, including condensation within the blotting chamber and difficulties in maintaining a stable sample temperatures. Here, we address these challenges and suggest practical strategies to minimise condensation and reduce temperature fluctuations during the plunge-freezing of samples at elevated temperatures (>40 °C). By preheating equipment and reducing chamber humidity and blotting times, we can improve sample preservation and grid reproducibility. These considerations are then demonstrated on poly(N-isopropylacrylamide) microgels, which exhibit a volume phase transition due to temperature changes.

1. Introduction

Control over the practical process of plunge-freezing is pivotal for advancing cryo-electron microscopy (cryo-EM) as a characterisation and analysis tool, from investigating the structure of proteins (Nakane et al., 2020) and polymer systems (Pothula et al., 2019) to virus assembly (Luque and Castón, 2020) and drug delivery systems (KUNTSCHE et al., 2011). Vitrification, rapid cooling that transitions a substance from a liquid to an amorphous solid state, is crucial for preserving the native structure of specimens at a molecular level (Dubochet et al., 1988; Thompson et al., 2016; Iancu et al., 2007). Blotting the sample on a grid is the most common approach in cryo-EM sample preparation. A small 3–4 µl droplet of sample on an EM grid is blotted via filter paper to form a thin liquid film of the sample across the grid. This is then plunged frozen into a cryogen liquid to vitrify the sample (Dobro et al., 2010; Armstrong et al., 2020). Sample vitrification via blotting is a fundamentally challenging method; where identical preparation conditions can still lead to inconsistent results due to variations in filter paper contact and the fibrous nature of the filter paper itself (Armstrong et al., 2020). However, methods and developments for improving sample preparation and grid reproducibility have now become well-established in the literature (Marie Haynes and Myers, 2023; Weissenberger et al., 2021). This method has benefited from more autonomous approaches in recent years to improve grid reproducibility and ice thickness (Koning et al., 2022). The ideal cryo-EM grid should present itself with a uniformly thin, electron-transparent vitrified sample layer. This is typically aided by semi-automated blotting machines, including the Vitrobot from Thermo Fisher Scientific and EM GP2 from Leica, both offering blotting chamber temperatures between 4 and 60 °C. They can regularly be found in cryo-EM facilities and have well-defined procedures and methodologies for varying circumstances and sample requirements, especially in the life sciences field (Iancu et al., 2007; Hands-Portman and Bakker, 2022). While still primarily used for biological research, more work is being done to extend the method beyond structural biology, particularly in the field of material research (Li et al., 2020, 2024). Furthermore, as the accessibility and availability of cryo-EM has increased in recent years (Danev et al., 2019), there is an increasing interest in using the unique characteristics of sample preparation for cryo-EM in material analysis (Allen et al., 2015; Wirix et al., 2014). A current challenge in characterisation within the material science field is directly visualising temperature-responsive materials such as poly (N-isopropylacrylamide) (pNIPAM) microgels (Grau-Carbonell et al., 2023) and thermo-responsive copolymers (de Souza Melchiors et al., 2022). Understanding the behaviour of these materials above and below their lower critical solution temperature (LCST) is crucial for their development and application (Scheffold, 2020). Cryo-EM is uniquely

* Corresponding author.
E-mail address: lieberw@mpip-mainz.mpg.de (I. Lieberwirth).

https://doi.org/10.1016/j.micron.2024.103745
Received 20 August 2024; Received in revised form 11 November 2024; Accepted 12 November 2024
Available online 13 November 2024

positioned to provide direct visualisation of these materials in a native state and can reveal more detail than traditional dried TEM conditions (Parry et al., 2008). Maintaining a sample at a desired temperature, such as at an elevated temperature above its LCST and rapidly freezing via vitrification, can be a tool to visualise temperature-dependent morphological changes (de Souza Melchiors et al., 2022; Frederik et al., 1991). Many temperature-responsive materials have an LCST in the region of 30–40 °C, (Schild, 1992; Del Monte et al., 2021) making them particularly relevant for medical applications (Chandorkar et al., 2019). Here, we chose a Vitrobot blotting chamber and a sample temperature of 45 °C, which offers a temperature margin above the LCST. However, these elevated blotting chamber temperatures are less well documented compared to procedures for freezing at 4 °C, 20 °C, or 37 °C. The plunge-freezing of elevated temperature samples (PF-ETS) brings its own set of challenges, and it can be difficult to maintain sample integrity during vitrification with a heated sample and blotting chamber above 40 °C, while also achieving a uniform vitrified ice layer. When working at elevated temperatures and high humidity levels, water condenses onto all surfaces inside that chamber, including the tweezers and grid, with the potential for water to drop into the liquid ethane, rapidly heating it. Here, we test methodical approaches such as preheating equipment and optimising the controllable parameters of the Vitrobot, as we aim to manage the blotting chamber's condensation and blotting conditions. The proposed recommendations described in this work aim to enhance the quality and reproducibility of vitrified samples at elevated temperatures, thereby broadening the applicability of cryo-EM in fields such as materials science and biochemistry.

2. Results and discussion

In our testing, reducing condensation within the blotting chamber and preheating tools is the primary factor in successful PF-ETS and sample stability. Working with a blotting chamber at 45 °C and 80 % humidity, some condensation is present, but the chamber window remains clear, and there are no large water droplets. Between 80 % and 90 %, this slowly degrades, and above 90 %, visibility is drastically impaired due to condensation and large droplets of water form on the interior surfaces (Fig. 1, a). This presents the risk of pooling water dropping through the hole into the ethane cup. At 80–90 % humidity, this does not occur actively, and the chamber remains usable for longer. We investigated the stability of the Vitrobot chamber as it was increased from room temperature to 45 °C and 85 % humidity (Fig. 3b). It is good practice to first set the temperature and, once stable, then set the desired humidity level when using the Vitrobot; this preheating reduces the condensation build-up within the chamber. In addition, our test showed that condensation can build up on the Vitrobot tweezer arm during plunge freezing if it is retracted during the heating process. This can be reduced by having the arm extended (as though to apply tweezers) during the heating process. This process, from room temperature to being ready to plunge at 45 °C, takes around 45 minutes. Once stable at the desired settings, the door was opened to add the filter paper and the chamber recovered within 3 minutes. To further reduce condensation build-up, we preheated the pipette tips and tweezers with grids to 45 °C using a heat plate. When room-temperature tweezers were inserted into the chamber, water immediately condenses onto them; this effect is minimised by pre-warming the tweezers with grids attached, as condensation can also form on the grid itself before the sample is applied (Fig. 1b). As the tweezers and grid are preheated, when loaded into the chamber, there is no need to wait for temperature equilibration, allowing immediate sample application to the grid. This also reduces the time for possible condensation to form on the grid and tweezer.

This preheating of the tools is also important for sample stability. Temperature-responsive samples can exhibit rapid morphological changes (Sershen et al., 2005) with temperature variations, therefore, preheating eliminates any undesirable temperature jumps during pipetting. In our experiments, pipette tips are heated by placing them on the same heating plate as the samples. It's also possible to submerge the tips into a heated water or sample buffer solution.

A further consideration when PF-ETS is the selection of appropriate blotting parameters which is crucial to ensure thin, uniform ice layers, which are essential for high-resolution imaging (Glaeser et al., 2016). Herein, we evaluated the Vitrobot blotting setting, considering: blotting force, duration, and the properties of the blotting paper itself, here we used grade 595 filter paper supplied by Plano GmbH. Vitrobot settings vary from lab to lab and even machine to machine within labs. We present our settings adjustments for different temperature as a guide for fine-tuning individual machines. Continuing to use a temperature of 45 °C and 85 % humidity, we tested how different blotting times impact the final EM grid. Initial tests were conducted using an aqueous solution and or all experiments, the drain time was set to 0 s, the blot total to 1, and the blot force to 0. With a blot time of 4 seconds, at 45 °C, all grids were left empty with all the grids squares left without ice (Fig. 2). As blot time was reduced by half-second intervals, at 3 s or less, grid squares began to contain amorphous ice. Consistent amorphous ice was visible across the grid at blot times between 1.5 and 2.5 seconds with less than 1 s giving inconsistent results but usually very thick, non-transparent ice.

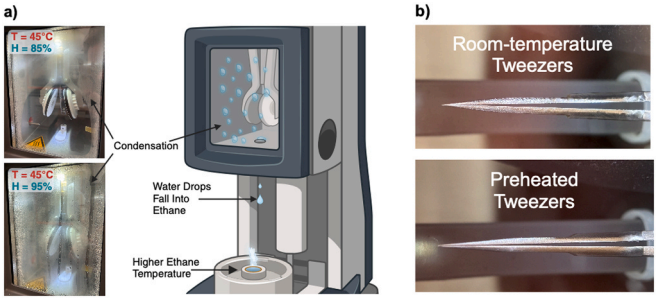

Fig. 1. a) Vitrobot model of various issues faced at elevated temperatures and live examples of the chamber at 45 °C with 80 % and 95 % humidity. b) Condensation on preheated and room-temperature tweezers in blotting chamber after 30 s in the chamber at 45 °C with 85 % humidity.

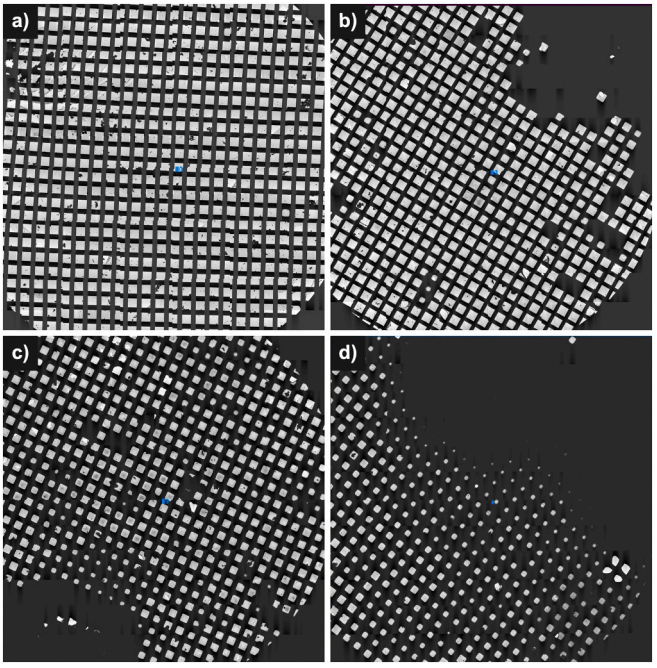

Fig. 2. Example grid maps. All grids were prepared with Vitrobot settings of 45 °C at 85 % humidity. Blot force 0 and blot total 1 for all girds. a) blot time 4 s b) blot time 3 s c) blot time 2 s d) blot time 1.5 s.

The reduction of blotting time at increased sample and atmospheric temperature is likely down to a decrease in viscosity (Kestin et al., 1978), a decrease in surface tension (Vargaftik et al., 1983) of the sample as well as potential evaporation (Glaeser et al., 2016) of the sample due to the elevated temperature and lower relative humidity. Table 1 represents our in-house guidance on Vitrobot settings.

The humidity and condensation can have implications for the blotting paper, which can become saturated, resulting in inconsistent blotting over time with the same settings. We looked to how the saturation level of the blotting paper varied with respect to the chamber environment. This was investigated by weighing the blotting paper in its dry state before being placed into the chamber. This was done for durations of 2, 5, 10, 15, 20, 25, and 30 min, across four distinct temperature and humidity settings (Fig. 3a). Following each exposure period, the blotting paper was promptly weighed again to ascertain the water content, indicated by the weight difference with each time interval repeated three times.

However, at 80 % humidity, the blotting paper did not saturate within the observation time. These results reflect the lack of saturation within the chamber due to the limited set humidity (85 % instead of 100 %). At 85 % humidity at 45 °C was found to have a similar saturation curve to that of a standard Vitrobot setting of 20 °C with 100 % humidity and ultimately offers a good balance between limiting the potential for sample evaporation and condensation.

In addition, we also examined the impact of different sample and chamber temperatures on the stability of the liquid ethane temperature. When preparing plunge-freezing samples, it is standard practice to maintain low liquid ethane temperatures, and when freezing with heated tweezers, extra care is needed to maintain the correct liquid ethane temperature. Ethane possesses a liquid phase between −183 °C and −90 °C and to avert the crystallisation of ice, liquid ethane must be maintained below the limit for the transition of amorphous ice to crystalline ice at around −145 °C (Dubochet et al., 1988). Our experiments involved measuring ethane's temperature at different chamber and sample temperatures 4 °C, 20 °C, and 45 °C (Fig. 3c). We found that the ethane's temperature remained safely below the point where crystalline ice forms, even after freezing up to 8 samples in a row when working at 4 and 20 °C. However, at increased chamber temperatures of 45 °C, after freezing 3 samples consecutively, the ethane began to warm. This was likely due to a combination of exposure to the warm chamber and the increased thermal energy of the tweezers. While this was still 10 °C below the point where crystallisation can occur, it reinforces that while freezing multiple samples, attention should be paid to the ethane temperature and recooling to near its freezing temperature after 2–3 samples. This is especially important at increased chamber and sample temperatures.

3. pNIPAM demonstration

After studying the variables of PF-ETS, we tested these methods on Poly(N-isopropylacrylamide) (pNIPAM) microgels. These are thermoresponsive hydrophilic polymer networks that exhibit a volume phase transition near the LCST, typically around 32 °C. Below the LCST, pNIPAM chains are hydrated, and the microgel particles are in a swollen state due to the predominance of hydrophilic interactions between the amide groups and water molecules. Upon heating above the LCST, intermolecular hydrogen bonding within the polymer network becomes more favourable compared to polymer-water interactions, leading to a hydrophobic collapse of the pNIPAM network, expelling water, and resulting in a significant decrease in the hydrodynamic radius of the microgel particles (Saunders and Vincent, 1999; Senff and Richtering, 1999). There have been ongoing investigations into the understanding and characterisation of this material (Scheffold, 2020; Shaulli et al., 2023). This temperature-dependent morphology makes pNIPAM microgels particularly suitable for this form of characterisation and thus as a test for the effectiveness of the previous findings. We used standard pNIPAM microgels with 5 mol% BIS, in a water solution. For imaging below the LCST, a temperature of 25 °C was used with a sample concentration of 5 mg/ml. For imaging above the LCST, the sample was then diluted to 2 mg/ml with water, as above the LCST the microgels collapse and become more hydrophobic. This transition increases hydrophobic interactions between particles, leading to a higher tendency for aggregation. Fig. 4 visualises the difference in the morphology of the temperature variation where at 25 °C, particles are in their swollen, hydrophilic state stabilising them, resulting in well-spaced particles. The diameter was found to be, on average, 600 nm with a standard deviation of 36 nm. The sample above its LCST was found to have an average diameter of 390 nm with a standard deviation of 38 nm and particles are closely packed due to their collapsed hydrophobic state reducing their stabilisation effect. By following the steps previously set out, it was possible to freeze samples with a grid quality matching that of lower temperatures and maintain sample integrity and grid quality.

Table 1
Optimised Vitrobot blotting settings for different temperatures. Blot Force 0 as calibrated by TFS.

Temperature (°C)	Humidity (%)	Blot Time (s)
4	100	4–5
20	100	4
30	95	3
45	85–90	1.5–2.5
55	85–90	1–2

4. Experimental methods

4.1. Vitrobot atmosphere monitoring

The experiment took place over 45 min with a starting temperature of 22 °C and 37 % humidity. The Vitrobot atmospheric temperature was accurately measured by independent temperature probes situated inside the chamber as well as the Vitrobot internal sensors. Measurements of temperature and humidity were taken at 30 s intervals. The values displayed by the Vitrobot were also recorded at the same time points as the measurements taken by the probe. Here, we see that it takes around 15 minutes for the chamber to reach the second condition, with the Vitrobot reading significantly lower temperatures until it stabilises. At 20 min, the door was opened for a total of 15 s to change the blotting paper, which was a chance to wipe away any condensation. While there is a small drop in temperature and a large drop in humidity, the chamber recovers within 2 min, meaning that changing blotting paper is very achievable by freezing multiple samples to avoid long-term build-up of condensation and possible blotting paper saturation.

4.2. Ethane temperature

Ethane temperature was measured with a temperature probe calibrated to −100 °C and capable of measuring down to −200 °C. The probe was cooled with liquid nitrogen in advance to minimise the temperature delta between the probe and ethane. Between the measurements, the probe was in a nitrogen atmosphere, maintaining a temperature of around −180 °C, again minimising the effect of the probe on the ethane. The probe was inserted into the ethane cup before and after each grid vitrification marked as a 'single run'. For consecutive runs, the initial ethane temperature was measured and then remeasured after 3 consecutive grid vitrification with no additional ethane cooling in between. Each experiment was repeated 3 times to acquire the range of ethane temperatures.

4.3. PNIPAM synthesis

pNIPAM microgels were synthesized with 5 mol% BIS using the free

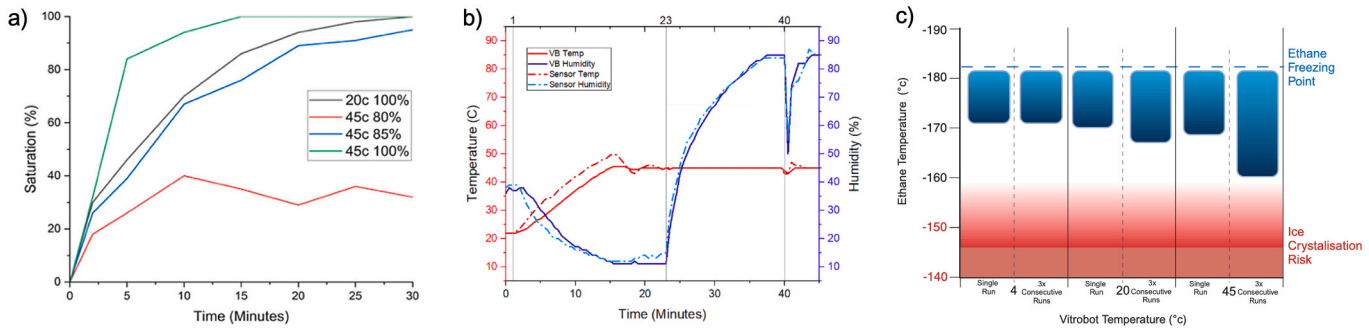

Fig. 3. a) Blotting paper saturation over time at 20 °C 100 % humidity and 45 °C at 80, 85 and 100 % humidity expressed as a percentage of the blotting paper's maximum potential weight gain, representing the total saturation level relative to the atmospheric conditions within the chamber. The maximum saturation of the blotting paper was calculated by leaving the blotting paper in the chamber at 100 % humidity for 1 h at the different measuring temperatures b) Monitoring of Vitrobot IV temperature and humidity where dashed lines represent the Vitrobot display and solid lines represent the true chamber conditions measured by a probe at the position of the grid. 45 °C set at t=1 min, 85 % humidity set at t=23 min and the door was opened for 15 s to add filter paper. c) Ethane temperature range before and after grid vitrification after a single grid 'Single Run' and after 3 consecutive grids 'Consecutive Runs'.

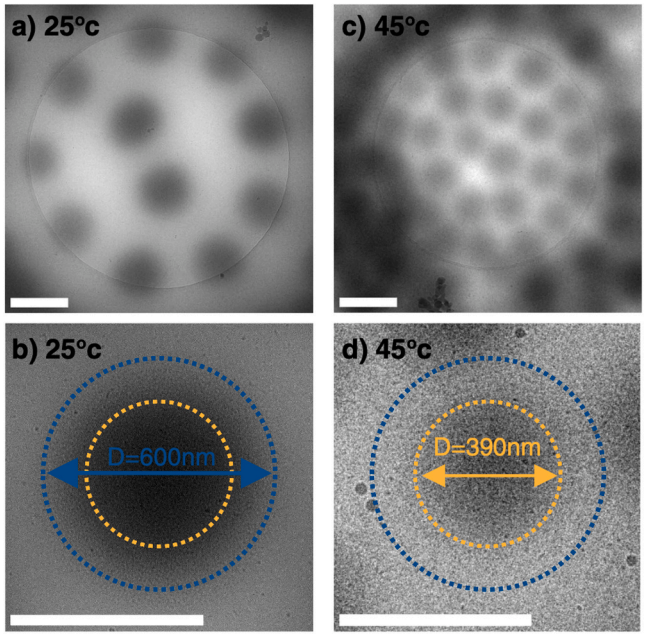

***Fig.* 4.** Cryo-EM micrographs of pNIPAM 5 % BIS a) 5 mg/ml vitrified at 25 °C. Total dose < 6e/Å^2, defocus −6 μm. b) Single microgel particle at 25 °C with an average particle diameter of 600 nm represented with a blue outline and a red outline representing the average diameter of the microgel particle at 45 °C. Total dose < 12e/Å^2, defocus −6 μm. c) 2 mg/ml vitrified at 45 °C. Total dose < 6e/Å^2, defocus −8 μm d) Single microgel particle at 45 °C with an average particle diameter of 390 nm represented with red outline and in blue the diameter of the gel at 25 °C. Scale bar 500 nm. Total dose < 12e/Å^2, defocus −8 μm.

radical precipitation polymerization method. N-isopropylacrylamide (Acros Organics, 99 %), NIPAM, is the monomeric unit that is recrystallized in hexane before use, and N,N-methylene bis(acrylamide) (Sigma–Aldrich, 99 %), BIS, is the cross-linker. In addition, N-(3-aminopropyl) methacrylamide hydrochloride (Polysciences), APMA, is added as a co-monomer to incorporate free amine groups into the microgel network. 2,2-Azobis(2-methylpropionamidine) dihydrochloride (Sigma–Aldrich, 98 %), AAPH, is used to initiate the polymerization. First, in a three-neck round bottom flask, NIPAM (1.430 g), BIS (0.099 g), and 5 ml of APMA previously prepared (0.01205 g in 15 ml H_2O) were dissolved in 85 g H2O. The reaction mixture was purged with nitrogen for 30 min before the temperature was raised to 70 °C. Next, 0.0365 g AAPH, previously dissolved in 5 ml H2O, was added to the reaction mixture. One minute after the initiator was added and the solution had started to turn white, the rest of the APMA solution was introduced to the reaction using a syringe pump at an addition rate of 0.5 ml/min. The reaction mixture was kept at 70 °C for 4 h before cooling down rapidly in an ice bath. Following this protocol, soft thermoresponsive microgels with 5 mol% crosslinker were obtained with the presence of amine groups throughout the microgel network that could serve for fluorescently labeling the microgels. A purification step follows to remove all unreacted monomers in the solution by centrifugation (3–4 times).

4.4. PNIPAM vitrification & imaging

For 25 °C – 3 μl of the sample was placed onto a quantifoil 2/1 400 mesh copper grid (previously glow discharged). The grid was then blotted for 4 s, plunged into liquid ethane (Vitrobot) and transferred into liquid nitrogen.

For 45 °C – The sample was preheated to 45 °C for 30 min prior to vitrification. Pipette tips were also placed into this heater. 3 μl of the sample was placed onto a quatrefoil 2/1 400 mesh copper grid (previously glow discharged). The grid was then blotted for 2 s, plunged into liquid ethane (Vitrobot) and transferred into liquid nitrogen.

Grids were then placed into a Cryo-TEM (Titan Krios G4, ThermoFisher Scientific). The TEM was operated at 300 kV and a 70 μm objective aperture. Micrographs were acquired using a Gatan K3 detector with a 20 eV filter-slit setting via serialEM. Size measurements were carried out by hand in ImageJ over 50 microgel particles at each temperature.

5. Conclusion

We propose a framework of guidelines and best practices to support advanced material characterisation in cryo-EM by utilising PF-ETS. Reducing the chamber humidity at elevated temperatures and reducing blotting times, resulted in amorphous grids while minimising the negative effects of condensation. Furthermore, preheating pipette tips and tweezers is an essential step to maintain sample integrity while also reducing further condensation. Although the Vitrobot was utilised as a reference system in this work, the procedures of preheating, blotting and chamber adjustments can be translated onto various vitrification devices. By improving the quality and reliability of vitrified samples kept at elevated temperatures before freezing, we aim to broaden the applicability of cryo-EM's applicability in fields like biochemistry and materials science to tackle the limitations in characterising temperature-responsive samples under conditions that more closely resemble their natural environments. This broadened scope allows for the examination

of materials and biological processes that are active at temperatures above the established blotting chamber temperatures.

CRediT authorship contribution statement

Iain Harley: Writing – review & editing, Writing – original draft, Visualization, Project administration, Methodology, Investigation, Data curation, Conceptualization. **Xhorxhina Shaulli:** Writing – review & editing, Validation, Resources, Investigation, Data curation. **Francesca Mazzotta:** Writing – review & editing, Validation, Methodology. **Katharina Landfester:** Writing – review & editing, Supervision, Resources. **Frank Scheffold:** Writing – review & editing, Supervision, Resources. **Ingo Lieberwirth:** Writing – review & editing, Writing – original draft, Supervision, Resources, Project administration.

Declaration of Competing Interest

The authors declare that they have no known competing financial interests or personal relationships that could have appeared to influence the work reported in this paper.

Acknowledgments

This project has received funding from the European Union's Horizon 2020 research and innovation programme under the Marie Skłodowska-Curie grant agreement SuperCol (no. 860914). Figures were created with BioRender.com.

Data availability

Data will be made available on request.

References

Allen, F.I., Comolli, L.R., Kusoglu, A., Modestino, M.A., Minor, A.M., Weber, A.Z., 2015. Morphology of hydrated as-cast nafion revealed through cryo electron tomography. ACS Macro Lett. 4 (1), 1–5. https://doi.org/10.1021/MZ500606H/SUPPL_FILE/MZ500606H_SI_001.PDF.

Armstrong, M., Han, B.G., Gomez, S., Turner, J., Fletcher, D.A., Glaeser, R.M., 2020. Microscale fluid behavior during Cryo-EM sample blotting. Biophys. J. 118 (3), 708–719. https://doi.org/10.1016/J.BPJ.2019.12.017.

Chandorkar, Y., Castro Nava, A., Schweizerhof, S., Van Dongen, M., Haraszti, T., Köhler, J., Zhang, H., Windoffer, R., Mourran, A., Möller, M., De Laporte, L., 2019. Cellular responses to beating hydrogels to investigate mechanotransduction. Nat. Commun. 2019 101 10 (1), 1–13. https://doi.org/10.1038/s41467-019-11475-4.

Danev, R., Yanagisawa, H., Kikkawa, M., 2019. Cryo-electron microscopy methodology: current aspects and future directions. Trends Biochem. Sci. 44 (10), 837–848. https://doi.org/10.1016/j.tibs.2019.04.008.

Del Monte, G., Truzzolillo, D., Camerin, F., Ninarello, A., Chauveau, E., Tavagnacco, L., Gnan, N., Rovigatti, L., Sennato, S., Zaccarelli, E., 2021. Two-step deswelling in the volume phase transition of thermoresponsive microgels. Proc. Natl. Acad. Sci. U. S. A 118 (37), e2109560118. https://doi.org/10.1073/PNAS.2109560118/SUPPL_FILE/PNAS.2109560118.SAPP.PDF.

Dobro, M.J., Melanson, L.A., Jensen, G.J., McDowall, A.W., 2010. Plunge freezing for electron cryomicroscopy. Methods Enzym. 481 (C), 63–82. https://doi.org/10.1016/S0076-6879(10)81003-1.

Dubochet, J., Adrian, M., Chang, J.-J., Homo, J.-C., Lepault, J., McDowall, A.W., Schultz, P., 1988. Cryo-electron microscopy of vitrified specimens. Q. Rev. Biophys. 21 (2), 129–228. https://doi.org/10.1017/S0033583500004297.

Frederik, P.M., Stuart, M.C.A., Bomans, P.H.H., Busing, W.M., Burger, K.N.J., Verkleij, A. J., 1991. Perspective and limitations of cryo-electron microscopy. J. Microsc. 161 (2), 253–262. https://doi.org/10.1111/j.1365-2818.1991.tb03088.x.

Glaeser, R.M., Han, B.G., Csencsits, R., Killilea, A., Pulk, A., Cate, J.H.D., 2016. Factors that influence the formation and stability of thin, cryo-EM specimens. Biophys. J. 110 (4), 749–755. https://doi.org/10.1016/j.bpj.2015.07.050.

Grau-Carbonell, A., Hagemans, F., Bransen, M., Elbers, N.A., van Dijk-Moes, R.J.A., Sadighikia, S., Welling, T.A.J., van Blaaderen, A., van Huis, M.A., 2023. In situ single particle characterization of the themoresponsive and co-nonsolvent behavior of PNIPAM Microgels and silica@PNIPAM core-shell colloids. J. Colloid Interface Sci. 635, 552–561. https://doi.org/10.1016/J.JCIS.2022.12.116.

Hands-Portman, I., Bakker, S.E., 2022. Customising the plunge-freezing workflow for challenging conditions. Faraday Discuss. 240, 44. https://doi.org/10.1039/D2FD00060A.

Iancu, C.V., Tivol, W.F., Schooler, J.B., Dias, D.P., Henderson, G.P., Murphy, G.E., Wright, E.R., Li, Z., Yu, Z., Briegel, A., Gan, L., He, Y., Jensen, G.J., 2007. Electron cryotomography sample preparation using the vitrobot. Nat. Protoc. 1 (6), 2813–2819. https://doi.org/10.1038/nprot.2006.432.

Kestin, J., Sokolov, M., Wakeham, W.A., 1978. Viscosity of liquid water in the range −8 °C to 150 °C. J. Phys. Chem. Ref. Data 7 (3), 941–948. https://doi.org/10.1063/1.555581.

Koning, R.I., Vader, H., van Nugteren, M., Grocutt, P.A., Yang, W., Renault, L.L.R., Koster, A.J., Kamp, A.C.F., Schwertner, M., 2022. Automated vitrification of Cryo-EM samples with controllable sample thickness using suction and real-time optical inspection. Nat. Commun. 13 (1), 2985. https://doi.org/10.1038/s41467-022-30562-7.

KUNTSCHE, J., HORST, J.C., BUNJES, H., 2011. Cryogenic transmission electron microscopy (Cryo-TEM) for studying the morphology of colloidal drug delivery systems. Cryog. Transm. Electron Microsc. Cryo-TEM Stud. Morphol. Colloïd. Drug Deliv. Syst. 417 (1–2), 120–137.

Li, W., Weng, S., Su, D., Wang, X., 2024. Expanding the cryogenic electron microscopy from biology to materials science. Renewables 2 (1), 73–87. https://doi.org/10.31635/RENEWABLES.024.202300046.

Li, Y., Huang, W., Li, Y., Chiu, W., Cui, Y., 2020. Opportunities for cryogenic electron microscopy in materials science and nanoscience. ACS Nano 14 (8), 9263–9276. https://doi.org/10.1021/ACSNANO.0C05020/ASSET/IMAGES/MEDIUM/NN0C05020_0005.GIF.

Luque, D., Castón, J.R., 2020. Cryo-electron microscopy for the study of virus assembly. Nat. Chem. Biol. 16 (3), 231–239. https://doi.org/10.1038/s41589-020-0477-1.

Marie Haynes, R., Myers, J.B., 2023. Expediting cryo-EM sample preparation using design of experiments. Biophys. J. 122 (3), 544a. https://doi.org/10.1016/j.bpj.2022.11.2879.

Nakane, T., Kotecha, A., Sente, A., McMullan, G., Masiulis, S., Brown, P.M.G.E., Grigoras, I.T., Malinauskaite, L., Malinauskas, T., Miehling, J., Uchański, T., Yu, L., Karia, D., Pechnikova, E.V., de Jong, E., Keizer, J., Bischoff, M., McCormack, J., Tiemeijer, P., Hardwick, S.W., Chirgadze, D.Y., Murshudov, G., Aricescu, A.R., Scheres, S.H.W., 2020. Single-particle Cryo-EM at atomic resolution. Nature 587 (7832), 152–156. https://doi.org/10.1038/s41586-020-2829-0.

Parry, A.L., Bomans, P.H.H., Holder, S.J., Sommerdijk, N.A.J.M., Biagini, S.C.G., 2008. Cryo electron tomography reveals confined complex morphologies of tripeptide-containing amphiphilic double-comb diblock copolymers. Angew. Chem. Int. Ed. 47 (46), 8859–8862. https://doi.org/10.1002/ANIE.200802834.

Pothula, K.R., Smyrnova, D., Schröder, G.F., 2019. Clustering Cryo-EM images of helical protein polymers for helical reconstructions. Ultramicroscopy 203, 132–138. https://doi.org/10.1016/j.ultramic.2018.12.009.

Saunders, B.R., Vincent, B., 1999. Microgel particles as model colloids: theory, properties and applications. Adv. Colloid Interface Sci. 80 (1), 1–25. https://doi.org/10.1016/S0001-8686(98)00071-2.

Scheffold, F., 2020. Pathways and challenges towards a complete characterization of microgels. Nat. Commun. 2020 111 11 (1), 1–13. https://doi.org/10.1038/s41467-020-17774-5.

Schild, H.G., 1992. Poly(N-Isopropylacrylamide): experiment, theory and application. Prog. Polym. Sci. 17 (2), 163–249. https://doi.org/10.1016/0079-6700(92)90023-R.

Senff, H., Richtering, W., 1999. Temperature sensitive microgel suspensions: colloidal phase behavior and rheology of soft spheres. J. Chem. Phys. 111 (4), 1705–1711. https://doi.org/10.1063/1.479430.

Sershen, S.R., Mensing, G.A., Ng, M., Halas, N.J., Beebe, D.J., West, J.L., 2005. Independent optical control of microfluidic valves formed from optomechanically responsive nanocomposite hydrogels. Adv. Mater. 17 (11), 1366–1368. https://doi.org/10.1002/ADMA.200401239.

Shaulli, X., Rivas-Barbosa, R., Bergman, M.J., Zhang, C., Gnan, N., Scheffold, F., Zaccarelli, E., 2023. Probing temperature responsivity of microgels and its interplay with a solid surface by super-resolution microscopy and numerical simulations. ACS Nano 17 (3), 2067–2078. https://doi.org/10.1021/ACSNANO.2C07569/ASSET/IMAGES/LARGE/NN2C07569_0007.JPEG.

de Souza Melchiors, M., Ivanov, T., Harley, I., Sayer, C., Araújo, P.H.H., Caire da Silva, L., Ferguson, C.T.J., Landfester, K., 2022. Membrane manipulation of giant unilamellar polymer vesicles with a temperature-responsive polymer. Angew. Chem. Int. Ed. 61 (39). https://doi.org/10.1002/anie.202207998.

Thompson, R.F.; Walker, M.; Siebert, C.A.; Muench, S.P.; Ranson, N.A. An Introduction to Sample Preparation and Imaging by Cryo-Electron Microscopy for Structural Biology. 2016. https://doi.org/10.1016/j.ymeth.2016.02.017.

Vargaftik, N.B., Volkov, B.N., Voljak, L.D., 1983. International tables of the surface tension of water. J. Phys. Chem. Ref. Data 12, 817. https://doi.org/10.1063/1.555688.

Weissenberger, G., Henderikx, R.J.M., Peters, P.J., 2021. Understanding the invisible hands of sample preparation for cryo-EM. Nat. Methods 18 (5), 463–471. https://doi.org/10.1038/S41592-021-01130-6.

Wirix, M.J.M., Bomans, P.H.H., Friedrich, H., Sommerdijk, N.A.J.M., De With, G., 2014. Three-dimensional structure of P3HT assemblies in organic solvents revealed by cryo-TEM. Nano Lett. 14 (4), 2033–2038. https://doi.org/10.1021/NL5001967/SUPPL_FILE/NL5001967_SI_002.MPG.